Latin American Journal of Solids and Structures
www.lajss.org

3On the use of finite strip method for buckling analysis of moderately thick plate by refined plate theory and using new types of functions

Abstract

A numerical method is developed for the buckling analysis of moderately thick plate with different boundary conditions. The procedure use the finite strip method in conjunction with the refined plate theory (RPT). Various refined shear displacement models are employed and compared with each other. These models account for parabolic, hyperbolic, exponential, and sinusoidal distributions of transverse shear stress, and they satisfy the condition of no transverse shear stress at the top and bottom surfaces of the plates without using a shear correction factor. The number of independent unknown functions involved here is only four, as compared to five functions in the shear deformation theories of Mindlin and Reissner. The numerical results of present theory are compared with the results of the first-order and the other higher-order theories reported in the literature. From the obtained results, it can be concluded that the present study predicts the behavior of rectangular plates with good accuracy.

Keywords

Refined plate theory; buckling analysis; finite strip method; shear deformation plate theories.

Saeed Mirzaei[a]
Mojtaba Azhari[b*]
Hossein Ali Rahimi Bondarabady[c]

[a,c]Department of Civil Engineering, Yazd University, Yazd, Iran
saeedmirzaei18@yahoo.com
h_rahimi@yazd.ac.ir
[b]Department of Civil Engineering, Isfahan University of Technology, Isfahan, Iran, 84156-83111

Corresponding author:
*mojtaba@cc.iut.ac.ir

http://dx.doi.org/10.1590/1679-78251280

Received 12.04.2014
In revised form 22.09.2014
Accepted 21.10.2014
Available online 30.10.2014

1 INTRODUCTION

The buckling behavior of orthotropic and laminated composite plates has been extensively studied, and various plate theories have been developed on the basis of transverse shear deformation effect.

The classical plate theory (CPT), which totally disregards the transverse shear deformation effect, provides reasonable results for thin plates (Das, 1963; Harik and Ekambaram, 1988; Bao et al., 1997; Leissa and Kang, 2002, 2005; Eisenberger and Alexandrov, 2003; Hwang and Lee, 2006; Ovesy et al., 2012); however, for moderately thick plates, it underestimates the deflections and

overestimates the buckling loads and natural frequencies. To overcome this shortcoming of the CPT, many shear deformation plate theories, which account for the transverse shear deformation effects, have been developed including the first-order shear deformation theory (FSDT) developed by Reissner (1945); Mindlin (1951). The FSDT accounts for the transverse shear deformation effect, but requires a shear correction factor to satisfy the stress-free conditions at the top and bottom surfaces of the plate (Dawe and Roufaeil, 1978; Wang et al., 2001; Bui and Rondal, 2008). Although the FSDT provides a sufficiently accurate description of response for thin to moderately-thick plates, it is not convenient to use due to the difficulty of determining an accurate shear correction factor. Thus, to avoid the use of a shear correction factor, many higher-order shear deformation plate theories (HSDTs) were proposed, including the theories of Reddy (1984); Ambartsumian (1958); Levinson (1980); Murthy (1981); Kaczkowski (1968); Panc (1975); Karama et al. (2009, 2003); Mantari et al. (2012); Zenkour (2005); Mechab et al. (2012); Touratier (1991); Benyoucef et al. (2010); Atmane et al. (2010); Soldatos (1992). Although the HSDTs with five unknowns provided sufficiently accurate results for thin to thick plate, their equations of motion were more complicated than those of the FSDT and CPT. Therefore, Shimpi (2002) developed a two-variable refined plate theory (RPT) which is simple to use. The Shimpi's theory is based on the assumption that the in-plane and transverse displacements consist of bending and shear components, and that the bending components do not contribute to shear forces and, likewise, the shear components do not contribute to bending moments. The most significant feature of this theory is that it applies transverse shear strains across the thickness as a quadratic function and satisfies the zero stress boundary conditions at the top and bottom surfaces of the plate without using a shear correction factor. Also, by having fewer unknowns in the equations, this theory enjoys a simpler form which is close to that of the classical plate theory. Some of the most important papers written based on this theory are:

Shimpi and Patel (2006a) extended the RPT to the vibration of isotropic plates. The RPT was applied to orthotropic plates by Shimpi and Patel (2006b) in the bending and vibration problems. Thai and Kim (2012, 2011) derived the Levy solution of the RPT for the bending, buckling, and vibration of orthotropic plates. Kim et al. (2009) derived the Navier solution of the RPT for the buckling of orthotropic plates. Vo and Thai (2012) adopted the RPT for the buckling and vibration analyses of laminated beams. Recently, the RPT has been extend to nanobeams (2012), nanoplates (2013, 2011), functionally graded sandwich plates (2011), and functionally graded plates (2012). Most of the studies based on the refined plate theory has been confined to the use of a particular function for the prediction of transverse shear deformation and have been conducted by using the Navier and Levy solutions.

In this paper, various simple higher-order shear deformation plate theories for the buckling of orthotropic and laminated composite plates are developed. These theories account for parabolic, hyperbolic, exponential, and sinusoidal distributions of transverse shear stress, and they satisfy the condition of no transverse shear stress at the top and bottom surfaces of the plates without using a shear correction factor. The number of unknown functions involved here is only four, compared to five functions in the case of shear deformation theories of Mindlin and Reissner which by removing this one unknown, we can save in the volume, time and cost of extra computations. The analysis employs the finite strip method. This method is applied to study the local instability of thick plates under compression with different boundary conditions. The numerical

results of present theory are compared with the results of the first-order and the other higher-order theories reported in the literature. This paper is organized into the following sections. In section 2, the different shear strain shape functions are presented and its application in the finite strip procedure is overviewed. Numerical results and discussions are presented in section 3. In section 4, some concluding remarks are highlighted.

2 THEORETICAL FORMULATION

2.1 Refined plate theory (Basic assumptions)

Consider the plate and a cartesian coordinate system as shown in Figure 1.

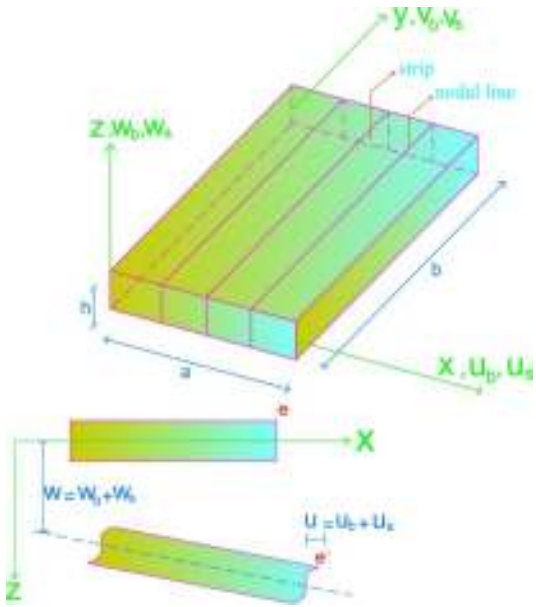


Figure 1: Illustrations of displacements and plate meshing arrangement.

The assumptions of the present theory are as follows:

i. The displacements are small in comparison with the plate thickness and, therefore, the resulting strains are infinitesimal.

ii. The transverse normal stress σ_z is negligible in comparison with the in-plane σ_x and σ_y.

iii. The transverse displacement w includes two components of bending w_b and shear w_s. These components are functions of coordinates x, y.

$$w(x,y,z) = w_b(x,y) + w_s(x,y) \tag{1}$$

iv. The in-plane displacements u and v consist of extension, bending, and shear components.

$$u = u_e + u_b + u_s \text{ and } v = v_e + v_b + v_s \tag{2}$$

The bending components u_b and v_b are assumed to be similar to the displacements given by the CPT. Therefore, the expressions for u_b and v_b are

$$u_b = -z\frac{\partial w_b}{\partial x} \text{ and } v_b = -z\frac{\partial w_b}{\partial y} \tag{3.a}$$

The shear components u_s and v_s, in conjunction with w_s, give rise to the $f_i(z)$ variations of shear strains γ_{xz}, γ_{yz} and hence to shear stresses σ_{xz}, σ_{yz} along the plate thickness h in such a way that shear stresses σ_{xz}, σ_{yz} are zero at the top and bottom surfaces of the plate. Consequently, u_s and v_s can be expressed as

$$u_s = f_i(z)\frac{\partial w_s}{\partial x} \text{ and } v_s = f_i(z)\frac{\partial w_s}{\partial y} \tag{3.b}$$

The objective of this paper is to develop various models to employ the new functions $f_i(z)$ for the buckling analysis of orthotropic and laminated composite plates under compression loading. These functions are shown in Table 1 and are depicted in Figure 2.

$f_i(z)$ function	Theory
$f_1(z) = \frac{z}{2}\left[\frac{h^2}{4} - \frac{z^2}{3}\right] - z$	Parabolic shear deformation theory (PSDT)
$f_2(z) = h\sinh\left(\frac{z}{h}\right) - z\cosh\left(\frac{1}{2}\right) - z$	Hyperbolic shear deformation theory (HSDT)
$f_3(z) = ze^{-2\left(\frac{z}{h}\right)^2} - z$	Exponential shear deformation theory (ESDT)
$f_4(z) = \frac{h}{\pi}\sin\left(\frac{\pi z}{h}\right) - z$	Sinusoidal shear deformation theory (SSDT)

Table 1: Different shear strain shape functions.

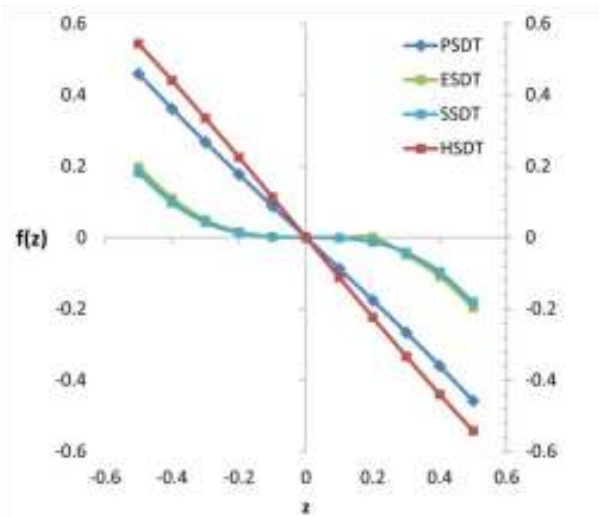


Figure 2: Variation of functions $f_i(z)$ along the plate thickness.

Functions $f_i(z)$ must be chosen to satisfy the following constraints:

$$\int_{-h/2}^{h/2} f_i(z)\,dz = 0, \quad \left.\frac{\partial f_i(z)}{\partial z}\right|_{z=\pm h/2} = -1 \tag{4}$$

2.2 Kinematics

Based on the assumptions made in the preceding section and using equations (1) through (3b), the displacement field can be obtained as

$$\begin{aligned} u(x,y,z) &= u_0(x,y) - z\frac{\partial w_b}{\partial x} + f_i(z)\frac{\partial w_s}{\partial x} \\ v(x,y,z) &= v_0(x,y) - z\frac{\partial w_b}{\partial y} + f_i(z)\frac{\partial w_s}{\partial y} \\ w(x,y,z) &= w_b(x,y) + w_s(x,y) \end{aligned} \tag{5}$$

where u and v are the in-plane displacements at any point $(x,\ y,\ z)$ in direction of x and y respectively; and u_0 and v_0 denote the in-plane displacements of point $(x,\ y,\ 0)$ on the mid-plane in x and y direction respectively, and $f_i(z)$ is placed from Table 1.

The kinematic relations can be obtained as follows:

$$\begin{Bmatrix} \varepsilon_x \\ \varepsilon_x \\ \gamma_{xy} \end{Bmatrix} = \begin{Bmatrix} \dfrac{\partial u}{\partial x} \\ \dfrac{\partial v}{\partial y} \\ \dfrac{\partial u}{\partial y} + \dfrac{\partial v}{\partial x} \end{Bmatrix} + z\begin{Bmatrix} -\dfrac{\partial^2 w_b}{\partial x^2} \\ -\dfrac{\partial^2 w_b}{\partial y^2} \\ -2\dfrac{\partial^2 w_b}{\partial x \partial y} \end{Bmatrix} + f(z)\begin{Bmatrix} \dfrac{\partial^2 w_s}{\partial x^2} \\ \dfrac{\partial^2 w_s}{\partial y^2} \\ 2\dfrac{\partial^2 w_s}{\partial x \partial y} \end{Bmatrix}, \begin{Bmatrix} \gamma_{yz} \\ \gamma_{xz} \end{Bmatrix} = g(z)\begin{Bmatrix} \dfrac{\partial w_s}{\partial y} \\ \dfrac{\partial w_s}{\partial x} \end{Bmatrix} \tag{6.a}$$

where

$$g(z) = \frac{df(z)}{dz} + 1 \tag{6.b}$$

2.3 Constitutive equations

It is assumed that the laminate is manufactured from orthotropic layers of pre-impregnated unidirectional fibrous composite materials (see Figure 3). Neglecting σ_z, the stress-strain relations for each layer in the (x,y,z) coordinate system may be written as

$$\begin{Bmatrix} \sigma_x \\ \sigma_y \\ \sigma_{xy} \\ \sigma_{yz} \\ \sigma_{xz} \end{Bmatrix} = \begin{bmatrix} Q_{11} & Q_{12} & 0 & 0 & 0 \\ Q_{12} & Q_{22} & 0 & 0 & 0 \\ 0 & 0 & Q_{66} & 0 & 0 \\ 0 & 0 & 0 & Q_{44} & 0 \\ 0 & 0 & 0 & 0 & Q_{55} \end{bmatrix} \begin{Bmatrix} \varepsilon_x \\ \varepsilon_y \\ \gamma_{xy} \\ \gamma_{yz} \\ \gamma_{xz} \end{Bmatrix} \tag{7}$$

where Q_{ij} are the plane stress-reduced stiffness values, which are known in terms of the engineering constants in the material axes of the layers:

$$Q_{11} = \frac{E_1}{1-\upsilon_{12}\upsilon_{21}},\ Q_{12} = \frac{\upsilon_{12}E_2}{1-\upsilon_{12}\upsilon_{21}},\ Q_{22} = \frac{E_2}{1-\upsilon_{12}\upsilon_{21}},\ Q_{66} = G_{12},\ Q_{44} = G_{23},\ Q_{55} = G_{13} \tag{8}$$

where E_1 and E_2 are the Young's moduli; υ_{12} and υ_{21} are the Poisson's ratios, and G_{12}, G_{23} and G_{13} are the shear moduli.

By performing a coordinate transformation, the stress-strain relations in the global coordinate system can be obtained as

$$\begin{Bmatrix}\sigma_x\\ \sigma_y\\ \sigma_{xy}\\ \sigma_{yz}\\ \sigma_{xz}\end{Bmatrix} = \begin{bmatrix}\bar{Q}_{11} & \bar{Q}_{12} & \bar{Q}_{16} & 0 & 0\\ \bar{Q}_{12} & \bar{Q}_{22} & \bar{Q}_{26} & 0 & 0\\ \bar{Q}_{16} & \bar{Q}_{26} & Q_{66} & 0 & 0\\ 0 & 0 & 0 & \bar{Q}_{44} & \bar{Q}_{45}\\ 0 & 0 & 0 & \bar{Q}_{45} & \bar{Q}_{55}\end{bmatrix}\begin{Bmatrix}\varepsilon_x\\ \varepsilon_y\\ \gamma_{xy}\\ \gamma_{yz}\\ \gamma_{xz}\end{Bmatrix} \tag{9}$$

and the compact form of Eq. (9) will be

$$\{\sigma\} = [\bar{Q}]\{\varepsilon\} \tag{10}$$

The components of $[\bar{Q}]$ for each laminated plate has been discussed by Reddy (2004).

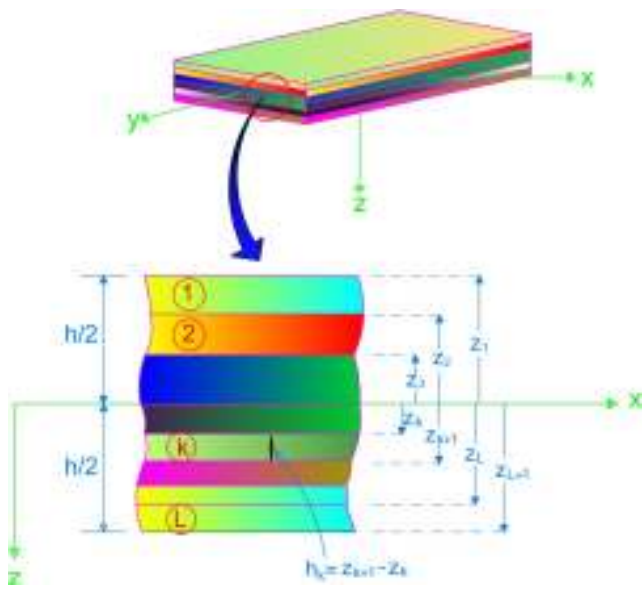


Figure 3: Coordinate system and layer numbering used for a typical laminated plate.

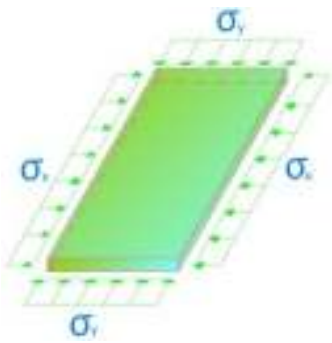


Figure 4: Pre-buckling stresses in a strip.

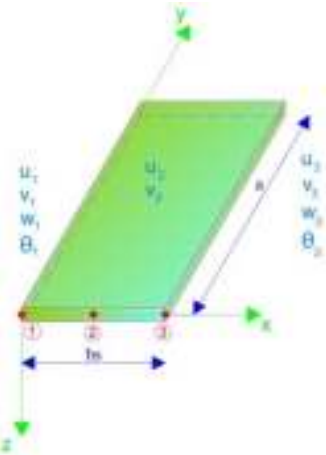


Figure 5: Pre-buckling system of displacements in a strip.

2.4 Finite strip method

In this section, the rectangular plate is modeled by a number of finite strips, each of which has three equally spaced nodal lines (see Figure 5) (Cheung, 1976). For the m^{th} harmonic, the displacement parameters of nodal line i are

$$\left\{\delta\right\}_{im} = \begin{Bmatrix} \left[u_{im}, v_{im}, w^b_{im}, \theta^b_{im}, w^s_{im}, \theta^s_{im}\right]^T, & \text{for } i = 1,3 \\ \left[u_{im}, v_{im}\right]^T, & \text{for } i = 2 \end{Bmatrix} \tag{11.a}$$

where

$$w^b = w_b, \quad w^s = w_s, \quad \theta^b = \frac{\partial w_b}{\partial x}, \quad \text{and} \quad \theta^s = \frac{\partial w_s}{\partial x} \tag{11.b}$$

The unknown displacement field functions (Eq. (5)) are assumed as follows:

$$u_0 = \sum_{m=1}^{r}\sum_{i=1}^{3} X\, S_m \left\{\delta\right\}_{im} \tag{12.a}$$

$$v_0 = \sum_{m=1}^{r}\sum_{i=1}^{3} Y\, S'_m \left\{\delta\right\}_{im} \tag{12.b}$$

$$w_b = \sum_{m=1}^{r}\sum_{i=1}^{3} R^b\, S_m \left\{\delta\right\}_{im} \tag{12.c}$$

$$w_s = \sum_{m=1}^{r}\sum_{i=1}^{3} R^s\, S_m \left\{\delta\right\}_{im} \tag{12.d}$$

in which

$$S'_m = \frac{d(S_m)}{dy} \tag{13}$$

where r is the number of harmonics and S_m is the m^{th} term of the basic function series (see Appendix) corresponding to particular end conditions, and X, Y, R^b, R^s are the interpolation matrices defined by Eq. (14).

$$X = \left[\frac{1}{2}\eta(\eta-1) \quad 0 \quad 0 \quad 0 \quad 0 \quad 0 \quad 1-\eta^2 \quad 0 \quad \frac{1}{2}\eta(\eta+1) \quad 0 \quad 0 \quad 0 \quad 0 \quad 0\right] \tag{14.a}$$

$$Y = \left[0 \quad \frac{1}{2}\eta(\eta-1) \quad 0 \quad 0 \quad 0 \quad 0 \quad 0 \quad 1-\eta^2 \quad 0 \quad \frac{1}{2}\eta(\eta+1) \quad 0 \quad 0 \quad 0 \quad 0\right] \tag{14.b}$$

$$R^b = \left[0 \quad 0 \quad \frac{1}{4}(1-\eta)^2(2+\eta) \quad \frac{b_s}{8}(1+\eta)(1-\eta)^2 \quad 0 \quad 0 \quad 0 \quad 0 \quad 0 \quad 0 \quad \frac{1}{4}(1+\eta)^2(2-\eta) \quad -\frac{b_s}{8}(1-\eta)(1+\eta)^2 \quad 0 \quad 0\right] \tag{14.c}$$

$$R^s = \left[0 \quad 0 \quad 0 \quad 0 \quad \frac{1}{4}(1-\eta)^2(2+\eta) \quad \frac{b_s}{8}(1+\eta)(1-\eta)^2 \quad 0 \quad 0 \quad 0 \quad 0 \quad 0 \quad 0 \quad \frac{1}{4}(1+\eta)^2(2-\eta) \quad -\frac{b_s}{8}(1-\eta)(1+\eta)^2\right] \tag{14.d}$$

In the above equations, $\eta = 2x/b_s$ and b_s is the strip width.

It should be noted that the Hermitian cubic polynomials used in the interpolation functions of w_b and w_s in the x direction, guarantee the inter-element continuity of the transverse displacement w and of its first derivatives $\partial w_b/\partial x$ and $\partial w_s/\partial x$. The linear and nonlinear buckling strain vectors $\{\varepsilon_L\}$ and $\{\varepsilon_{NL}\}$ are given by

$$\{\varepsilon_L\} = \left\{\frac{\partial u}{\partial x}; \frac{\partial v}{\partial y}; \frac{\partial u}{\partial y} + \frac{\partial v}{\partial x}; \frac{\partial w}{\partial y} + \frac{\partial v}{\partial z}; \frac{\partial w}{\partial x} + \frac{\partial u}{\partial z}\right\}^T \tag{15}$$

$$\{\varepsilon_{NL}\} = \begin{Bmatrix} \frac{1}{2}\left[\left(\frac{\partial u}{\partial x}\right)^2 + \left(\frac{\partial v}{\partial x}\right)^2 + \left(\frac{\partial w}{\partial x}\right)^2\right] \\ \frac{1}{2}\left[\left(\frac{\partial u}{\partial y}\right)^2 + \left(\frac{\partial v}{\partial y}\right)^2 + \left(\frac{\partial w}{\partial y}\right)^2\right] \\ \left[\frac{\partial u}{\partial x}\frac{\partial u}{\partial y} + \frac{\partial v}{\partial x}\frac{\partial v}{\partial y} + \frac{\partial w}{\partial x}\frac{\partial w}{\partial y}\right] \end{Bmatrix} \tag{16}$$

Using Eqs. (12a) through (12d) and (4) the linear strain vector $\{\varepsilon_L\}$ becomes

$$\{\varepsilon_L\} = \sum_{m=1}^{r}\sum_{i=1}^{3}[B]_{im}\{\delta\}_{im} \tag{17}$$

where $[B]_{im}$ is the strain matrix.

The total strain energy U stored during buckling may be written as

$$U = \frac{1}{2}\int_V \{\varepsilon_L\}^T\{\sigma\}dV \tag{18}$$

where V is the volume of the strip. Hence, by substituting Eqs. (10) and (17) into Eq. (18) the stiffness matrix is obtained from

$$U = \frac{1}{2}\{\delta\}_{im}^{T}[K]_{ijmn}\{\delta\}_{jn} \tag{19}$$

in which $[K]_{ijmn}$ is the stiffness matrix corresponding to nodal lines i and j, and it can be expressed as

$$[K]_{ijmn} = \int_{-\frac{h}{2}}^{\frac{h}{2}}\int_{0}^{b}\int_{-1}^{1}[B]_{im}^{T}[\overline{Q}][B]_{jn}\,dxdydz \tag{20}$$

where m and n denote the related series terms.

The strip is subjected to in-plane stresses σ_x and σ_y shown in Figure 4. The potential energy reduction of these stresses (V_p) during buckling is given by

$$V_p = \frac{1}{2}\int_V \{\varepsilon_{NL}\}^T\{\sigma\}dV \tag{21}$$

By appropriate substitution, the stability matrix $[K_G]$ can be obtained from

$$V = \frac{1}{2}\{\delta\}_{im}^{T}[K_G]_{ijmn}\{\delta\}_{jn} \tag{22}$$

in which

$$[K_G]_{ijmn} = \frac{1}{2}\int_V \left\{[G_u]_{im}^{T}[\sigma]^0[G_u]_{jn} + [G_v]_{im}^{T}[\sigma]^0[G_v]_{jn} + [G_w]_{im}^{T}[\sigma]^0[G_w]_{jn}\right\}dV \tag{23}$$

Where

$$\left\langle \frac{\partial u}{\partial x} + \frac{\partial u}{\partial y} \right\rangle = \sum_{m=1}^{r}\sum_{i=1}^{3}[G_u]_{im}\{\delta\}_{im} \tag{24.a}$$

$$\left\langle \frac{\partial v}{\partial x} + \frac{\partial v}{\partial y} \right\rangle = \sum_{m=1}^{r}\sum_{i=1}^{3}[G_v]_{im}\{\delta\}_{im} \tag{24.b}$$

$$\left\langle \frac{\partial w}{\partial x} + \frac{\partial w}{\partial y} \right\rangle = \sum_{m=1}^{r}\sum_{i=1}^{3}[G_w]_{im}\{\delta\}_{im} \tag{24.c}$$

and

$$[\sigma]^0 = \begin{bmatrix} \sigma_x^0 & \sigma_{xy}^0 \\ \sigma_{xy}^0 & \sigma_y^0 \end{bmatrix} \tag{25}$$

In the equations (24a-c), $[G_u]_{im}$, $[G_v]_{im}$ and $[G_w]_{im}$ are the stability matrices. Once the stiffness matrix $[K]_{ijmn}$ and stability matrix $[K_G]_{ijmn}$ have been derived, and combined for each com-

posite strip, they can be assembled into the respective global matrices $\left[K\right]$ and $\left[K_G\right]$ using standard procedures. The buckling problem can then be solved by eigenvalue equations

$$\left(\left[K\right]-\lambda\left[K_G\right]\right)\left\{\Delta\right\}=0 \tag{26}$$

where λ is a scaling factor related to the critical load and $\left\{\Delta\right\}$ is the eigenvector.

3 NUMERICAL RESULTS

The numerical program has been written in the MATLAB environment which can model various boundary conditions and three types of isotropic, orthotropic and laminated composite plates.
In this section, to verify the accuracy of the RPT in predicting the buckling behavior of orthotropic and asymmetric cross-ply laminates under different boundary conditions, various numerical examples are presented for laminates with the following properties, and the results of the RPT are compared with those of the classical plate theory (CPT), first-order shear deformation theory (FSDT) and higher-order shear deformation plate theory (HSDT). The explanations of various displacement models are given in Table 2.

Material type (1) Reddy (2004)

$E_1/E_2 = \text{varied}$, $G_{12}=G_{13}=0.5E_2$, $G_{23}=0.2E_2$, $\upsilon_{12}=0.25$

Material type (2) Reddy (2004)

$E_1/E_2 = \text{varied}$, $G_{12}=G_{13}=0.6E_2$, $G_{23}=0.5E_2$, $\upsilon_{12}=0.25$

To more conveniently present the numerical results in graphical and tabular forms, they are dimensionless using the following relation:

$$\bar{N}=N_{cr}\left(\frac{a^2}{E_2h^2}\right) \tag{27}$$

In obtaining the results, plate strips with 14 degrees of freedom have been used. Also in all the results, except the mentioned cases, one harmonic and 10 strips have been used.

In all the tables and figures, a, b and h are the plate width, length and thickness, respectively; and k is shear correction factor for the first-order shear deformation theory (FSDT).

Model	Theory	Unknowns
CPT	Classical plate theory	3
FSDT	First-order shear deformation theory	5
TSDT	Third-order deformation theory	5
Present PSDT	Parabolic shear deformation theory	4
Present HSDT	Hyperbolic shear deformation theory	4
Present ESDT	Exponential shear deformation theory	4
Present SSDT	Sinusoidal shear deformation theory	4

Table 2: Description of various displacement models.

3.1 Buckling analysis of simply-supported square orthotropic plate

The dimensionless buckling loads of the simply-supported square orthotropic plate ($a = b$) have been presented in Tables 3 and 4 as well as Figures 6, 8 and 9. Material type (1), 10 strips and the first harmonic are used. The results obtained from the RPT numerical solution agree well with the Kim's Navier solutions and the FSDT results. Also, the difference between the results of the present theory, FSDT ($k = 5/6$), and CPT have been illustrated in Figures 6 and 7 as an increase in the a/h ratio and in Figures 8 and 9 as an increase in the elasticity modulus. As shown in Table 3, the differences between the results of the present study and FSDT ($k = 5/6$), and between the results of the present study and FSDT ($k = 1$) are 15.42% and 1.6%, respectively, for the same case of square orthotropic plate ($a = b = 5h$ and $E_1/E_2 = 40$). The buckling load of a square orthotropic plate subjected to in-plane biaxial pressure was presented in Table 4 and Figure 7, which for converging the results, we used the first two harmonics (m =1 and m =2) and 10 strips. The first two buckling mode shapes of a simply supported square orthotropic plate boundary conditions and $a/h = 5$ and subjected to in-plane uniaxial compressive load is depicted in Figure 10.

b/h	Theories	Orthotropic		
		$E_1/E_2 = 10$	$E_1/E_2 = 25$	$E_1/E_2 = 40$
5	**Present** PSDT	**6.2126**	**9.0109**	**10.5133**
	Kim et al. (2009a)	6.3478	9.1039	10.5785
	FSDT $k = 2/3$	5.5679	7.1122	7.7411
	FSDT $k = 5/6$	6.1804	8.2199	9.1085
	FSDT $k = 1$	6.6715	9.1841	10.3463
10	**Present** PSDT	**9.2655**	**16.6319**	**22.1168**
	Kim et al. (2009a)	9.3732	16.7719	22.2581
	FSDT $k = 2/3$	8.8988	14.7011	18.3575
	FSDT $k = 5/6$	9.2733	15.8736	20.3044
	FSDT $k = 1$	95415	16.7699	21.8602
20	**Present** PSDT	**10.6138**	**21.2759**	**30.9730**
	Kim et al. (2009a)	10.6534	21.3479	31.0685
	FSDT $k = 2/3$	10.4926	20.4034	28.8500
	FSDT $k = 5/6$	10.6199	20.9528	30.0139
	FSDT $k = 1$	10.7066	21.3363	30.8451
50	**Present** PSDT	**11.0709**	**23.1080**	**34.9503**
	Kim et al. (2009a)	11.0780	23.1225	34.9717
	FSDT $k = 2/3$	11.0497	22.9366	34.4886
	FSDT $k = 5/6$	11.0721	23.0461	34.7487
	FSDT $k = 1$	11.0871	21.3363	34.9244
100	**Present** PSDT	**11.1398**	**23.3971**	**35.6067**
	Kim et al. (2009a)	11.1415	23.4007	35.6120
	FSDT $k = 2/3$	11.1343	23.3527	35.4852
	FSDT $k = 5/6$	11.1400	23.3810	35.5538
	FSDT $k = 1$	11.1438	23.3999	35.5996
	CPT	11.1628	23.4949	35.8307

Table 3: Nondimensional critical buckling loads of simply-supported (SSSS) square plates subjected to uniaxial compression.

b/h	Theories	Orthotropic		
		$E_1/E_2 = 10$	$E_1/E_2 = 25$	$E_1/E_2 = 40$
5	**Present** PSDT	**2.7453**[a]	**3.2417**[a]	**3.5995**[a]
	Kim et al. (2009a)	2.8549[a]	3.3309[a]	3.4800[a]
	FSDT $k = 2/3$	2.5042[a]	2.7332[a]	2.8303[a]
	FSDT $k = 5/6$	2.8319[a]	3.1422[a]	3.2822[a]
	FSDT $k = 1$	3.1027[a]	3.4933[a]	3.6793[a]
10	**Present** PSDT	**4.5555**	**5.9363**[a]	**7.1217**[a]
	Kim et al. (2009a)	4.6718	6.0646[a]	7.2536[a]
	FSDT $k = 2/3$	4.4259	5.4351[a]	6.0797[a]
	FSDT $k = 5/6$	4.6367	5.8370[a]	6.6325[a]
	FSDT $k = 1$	4.7708	6.1425[a]	7.0690[a]
20	**Present** PSDT	**5.3069**	**7.5993**[a]	**9.5835**[a]
	Kim et al. (2009a)	5.3267	7.6643[a]	9.6614[a]
	FSDT $k = 2/3$	5.2463	7.3701[a]	8.9895[a]
	FSDT $k = 5/6$	5.3100	7.5546[a]	9.3049[a]
	FSDT $k = 1$	5.3533	7.6834[a]	9.5297[a]
50	**Present** PSDT	**5.5355**	**8.2653**[a]	**10.6409**[a]
	Kim et al. (2009a)	5.5390	8.2784[a]	10.6576[a]
	FSDT $k = 2/3$	5.5249	8.2199[a]	10.5111[a]
	FSDT $k = 5/6$	5.5361	8.2566[a]	10.5810[a]
	FSDT $k = 1$	5.5436	8.2812[a]	10.6282[a]
100	**Present** PSDT	**5.5699**	**8.3710**[a]	**10.8129**[a]
	Kim et al. (2009a)	5.5707	8.3744[a]	10.8172[a]
	FSDT $k = 2/3$	5.5672	8.3593[a]	10.7788[a]
	FSDT $k = 5/6$	5.5700	8.3687[a]	10.7972[a]
	FSDT $k = 1$	5.5719	8.3751[a]	10.8095[a]
	CPT	5.5814	8.4069[a]	10.8715[a]

[a] (10 strips and first two harmonics)

Table 4: Nondimensional critical buckling loads of simply-supported (SSSS) square plates ($a = b$) subjected to biaxial compression.

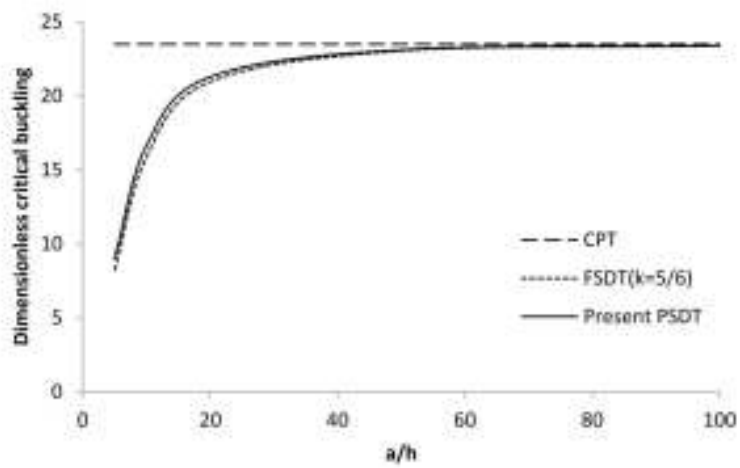


Figure 6: The effect of side-to-thickness ratio on the critical buckling load of square plates subjected to uniaxial compression; $E_1/E_2 = 25$.

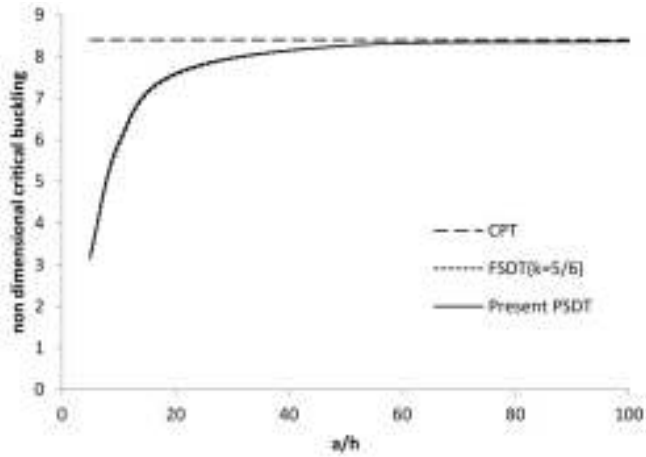


Figure 7: The effect of side-to-thickness ratio on the critical buckling load of square plates subjected to biaxial compression; $E_1/E_2 = 25$.

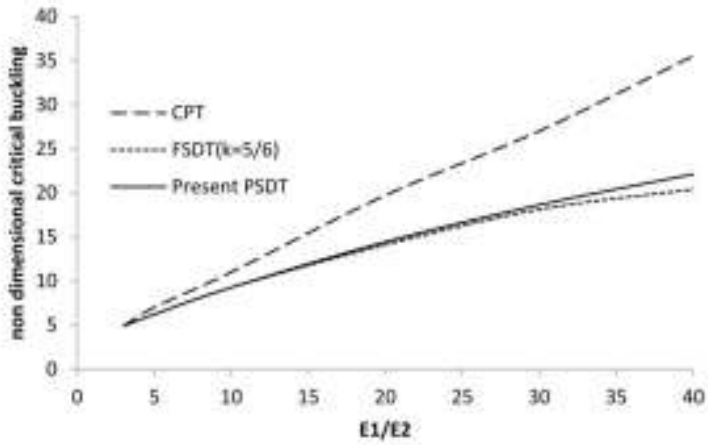


Figure 8: The effect of modulus ratio on the critical buckling load of square plates subjected to uniaxial compression; $a/h = 10$.

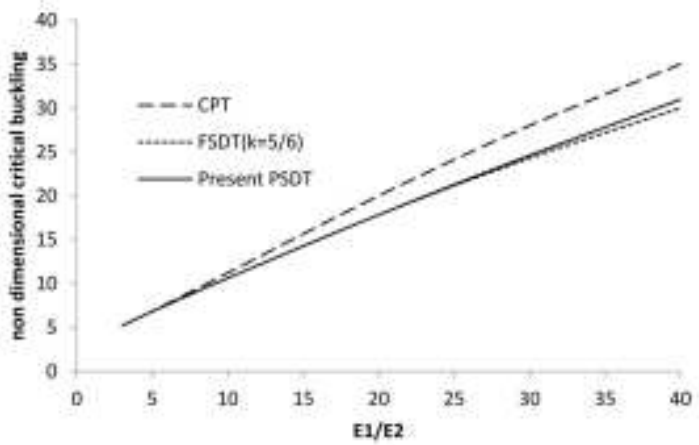


Figure 9: The effect of modulus ratio on the critical buckling load of square plates subjected to uniaxial compression; $a/h = 20$.

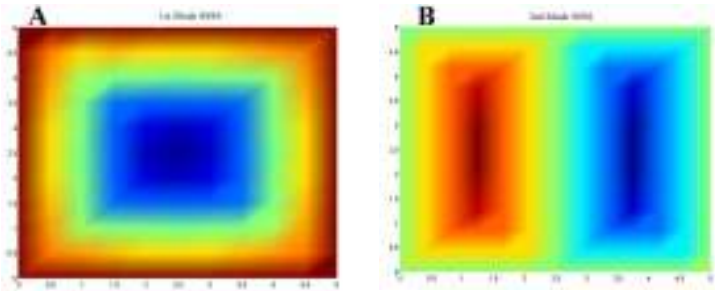


Figure 10: The first two buckling mode shapes of a square orthotropic plate with simply supported boundary conditions.

3.2 Buckling analysis of simply-supported square orthotropic plate with various shear deformation theories

Table 5 has listed the critical buckling loads obtained from various shear deformation theories for simply-supported orthotropic square plates subjected to uniaxial compression. Material type (1), 10 strips and the first harmonic are used to solve the problem. As shown in Table 5, the non-dimensional buckling loads obtained by sinusoidal and exponential functions are greater than those obtained by hyperbolic and parabolic functions.

b/h	**present** $f_i(z)$	Orthotropic		
		$E_1/E_2 = 10$	$E_1/E_2 = 25$	$E_1/E_2 = 40$
5	$f_1(z)$ (PSDT)	6.2126	9.0109	10.5133
	$f_2(z)$ (HSDT)	6.2122	9.0090	10.5094
	$f_3(z)$ (ESDT)	6.2390	9.0921	10.6577
	$f_4(z)$ (SSDT)	6.2637	9.0897	9.9596
	FSDT $k = 1$	6.6715	9.1841	10.3463
20	$f_1(z)$ (PSDT)	10.6138	21.2759	30.9730
	$f_2(z)$ (HSDT)	10.6138	21.2759	30.9729
	$f_3(z)$ (ESDT)	10.6168	21.2885	31.0011
	$f_4(z)$ (SSDT)	10.6253	21.3218	31.0692
	FSDT $k = 1$	10.7066	21.3363	30.8451
100	$f_1(z)$ (PSDT)	11.1398	23.3971	35.6067
	$f_2(z)$ (HSDT)	11.1398	23.3971	35.6067
	$f_3(z)$ (ESDT)	11.1399	23.3977	35.6080
	$f_4(z)$ (SSDT)	11.1402	23.3992	35.6116
	FSDT $k = 1$	11.1628	23.3999	35.5996

Table 5: Nondimensional critical buckling loads obtained by various $f_i(z)$ for simply-supported square plates subjected to uniaxial compression.

3.3 Buckling analysis of square orthotropic plate with different boundary conditions

The non-dimensional buckling loads of square orthotropic plates ($a = b$) with different boundary conditions have been shown in Table 6 and Figure 11. In this section, the boundary conditions of two loaded ends are simply supported and side edges boundary conditions are considered as sim-

ply supported, clamped and free. Material type (1), 10 strips and the first harmonic term is used to solve the problem. In Table 6, a comparison has been made between the critical buckling loads of thin plates ($a/h = 100$) achieved by the present RPT numerical solution, the Levy-Thai solution (2011) and the CPT solution. The changes of the critical buckling load with thickness ratio and PSDT model are shown in Figure 11. In Table 6, β_1 and β_2 are the load parameters that indicate the loading conditions. Positive values for β_1 and β_2 indicate that the plate is subjected to biaxial compressive loads. Also, a zero value for β_1 or β_2 shows uniaxial loading in the x or y direction, respectively. The buckling mode shapes of a square orthotropic plate with various boundary conditions and $a/h = 5$, subjected to in-plane uniaxial pressure are shown in Figure 12.

(β_1,β_2)	E_1/E_2	Method	Boundary condition			
			SSSS	*SSCC*	*SSSC*	*SSFF*
		Present PSDT	**11.1398**	**45.5671**	**23.3279**	**2.8190**
	10	Thai et al. (2011)	11.1415	45.5714	23.3315	2.8192
		CPT	11.1628	45.9207	23.4222	2.8206
		Present PSDT	**23.3971**	**107.3591**	**53.0498**	**2.8200**
(0,1)	25	Thai et al. (2011)	23.4007	107.3597	53.0572	2.8203
		CPT	23.4949	109.3141	53.5274	2.8216
		Present PSDT	**35.6067**	**167.8998**	**82.4827**	**2.8203**
	40	Thai et al. (2011)	35.6120	167.8887	82.4930	2.8206
		CPT	35.8307	172.7103	83.6346	2.8219
		Present PSDT	**5.5698**	**20.1498**	**10.7250**	**1.2742**
	10	Thai et al. (2011)	5.5707	20.1558	10.7273	1.2745
		CPT	5.5814	20.2904	10.7658	1.2750
		Present PSDT	**11.6984**	**47.4986**	**2403747**	**1.2735**
(1,1)	25	Thai et al. (2011)	11.7003	47.5122	24.3799	1.2737
		CPT	11.7475	48.2668	24.5792	1.2743
		Present PSDT	**17.8031**	**74.3589**	**37.9024**	**1.2732**
	40	Thai et al. (2011)	17.8060	74.3794	37.9103	1.2735
		CPT	17.9154	76.2450	38.3944	1.2741

Table 6: Comparison between nondimensional critical buckling loads of square orthotropic plates with different boundary conditions ($a/h = 100$).

3.4 Buckling analysis of simply-supported square asymmetric cross-ply laminated plate

The critical buckling loads of two-layer asymmetric cross-ply laminated plates under uniaxial and biaxial loadings are presented in Table 7 for modulus ratios $E_1/E_2 = 10, 25, 40$ and material type (1). In Tables 7 and 8 as well as Figure 13, 10 strips and the first harmonic term are used to solve the problem. In table 8, a simply-supported asymmetric cross-ply $(0/90)_n$ $(n = 2,3,5)$ square laminate subjected to uniaxial compressive load on sides $(x = 0,a)$ and with modulus ratios $E_1/E_2 = 40$ is considered. Material type (2) is used. Table 8 shows a comparison between the results obtained by using various models and the 3-D elasticity solutions given by Noor (1975). The results clearly indicate that the present theories predict the buckling loads more accurately than the identical HSDTs.

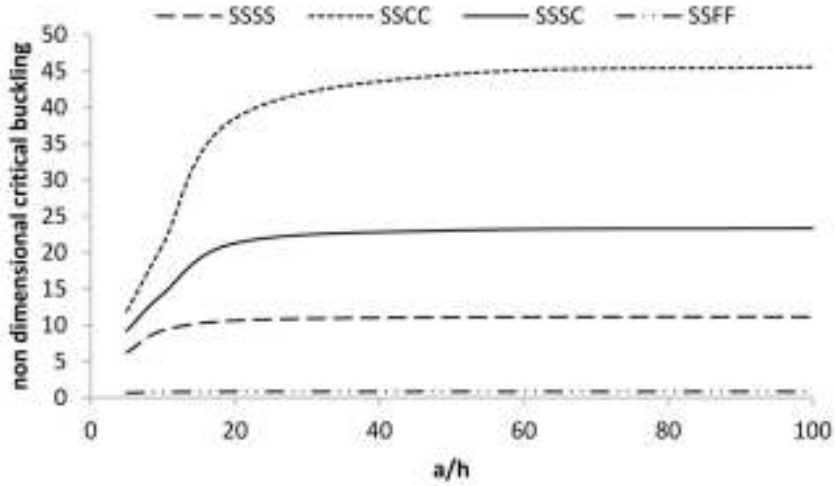


Figure 11: The effect of side-to-thickness ratio on the critical buckling load of square plates with different boundary conditions subjected to uniaxial compression along the y-axis; $E_1/E_2 = 10$ and PSDT model.

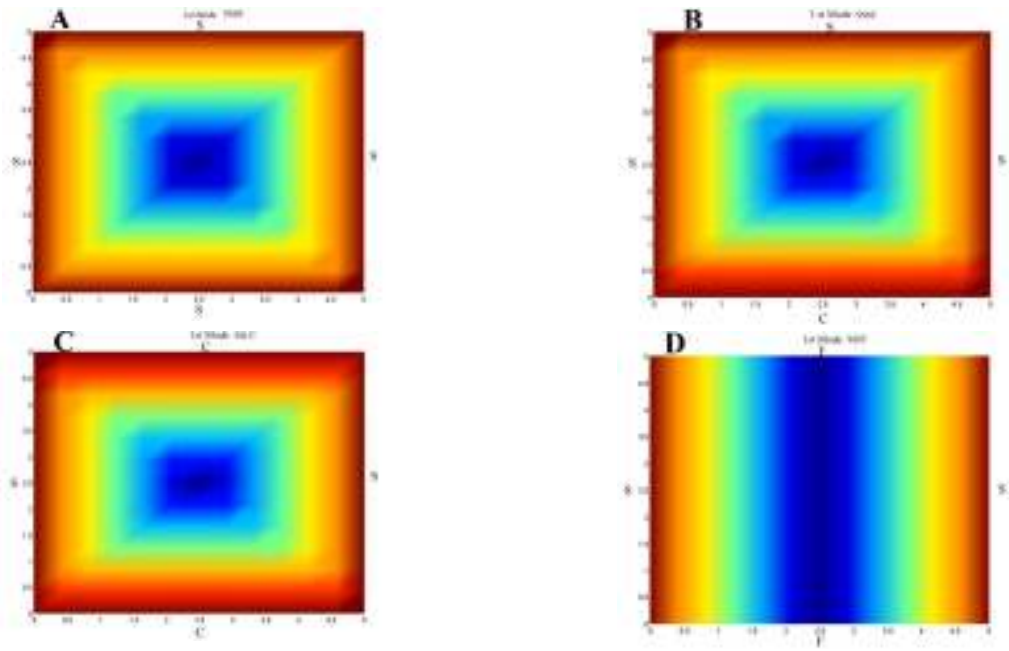


Figure 12: The buckling mode shapes of a square orthotropic plate with various boundary conditions; A: SSSS, B: SSSC, C: SSCC, D: SSFF

The effect of side-to-thickness ratio on the buckling load of simply-supported four-layer $(0\ /\ 90\ /\ 0\ /\ 90)$ square laminates has been presented in Figure 13 with modulus ratios $E_1/E_2 = 40$. Buckling mode shape of a square laminated composite plate (0/90/0/90) with simply supported boundary conditions and $a/h = 5$, subjected to in-plane uniaxial pressure have been illustrated in Figure 14.

b/h	Theories	(0 / 90)		
		$E_1/E_2 = 10$	$E_1/E_2 = 25$	$E_1/E_2 = 40$
Uniaxial Compression				
10	**Present** (PSDT)	**5.6641**	**8.1636**	**10.4671**
	Present (HSDT)	**5.6636**	**8.1620**	**10.4639**
	Present (SSDT)	**5.6645**	**8.1652**	**10.4705**
	Reddy (2004)	5.746	8.189	10.381
20	**Present** (PSDT)	**6.1777**	**9.1378**	**11.9961**
	Present (HSDT)	**6.1775**	**9.1373**	**11.9951**
	Present (SSDT)	**6.1778**	**9.1383**	**11.9972**
	Reddy (2004)	6.205	9.153	11.980
100	**Present** (PSDT)	**6.3662**	**9.5102**	**12.6016**
	Present (HSDT)	**6.3662**	**9.5101**	**12.6015**
	Present (SSDT)	**6.3662**	**9.5102**	**12.6016**
	Reddy (2004)	6.367	9.511	12.601
	CLPT	6.374	9.526	12.628
Biaxial Compression				
10	**Present** (PSDT)	**2.8319**	**4.0816**	**5.2333**
	Present (HSDT)	**2.8317**	**4.0808**	**5.2317**
	Present (SSDT)	**2.8321**	**4.0824**	**5.2350**
	Reddy (2004)	2.873	4.094	5.190
20	**Present** (PSDT)	**3.0888**	**4.5689**	**5.9980**
	Present (HSDT)	**3.0888**	**4.5686**	**5.9975**
	Present (SSDT)	**3.0889**	**4.5691**	**5.9986**
	Reddy (2004)	3.102	4.576	5.990
100	**Present** (PSDT)	**3.1831**	**4.7551**	**6.3008**
	Present (HSDT)	**3.1831**	**4.7551**	**6.3008**
	Present (SSDT)	**3.1831**	**4.7551**	**6.3008**
	Reddy (2004)	3.184	4.755	6.300
	CLPT	3.187	4.763	6.314

Table 7: Nondimensional critical buckling load of simply-supported asymmetric cross-ply square plates ($a = b$).

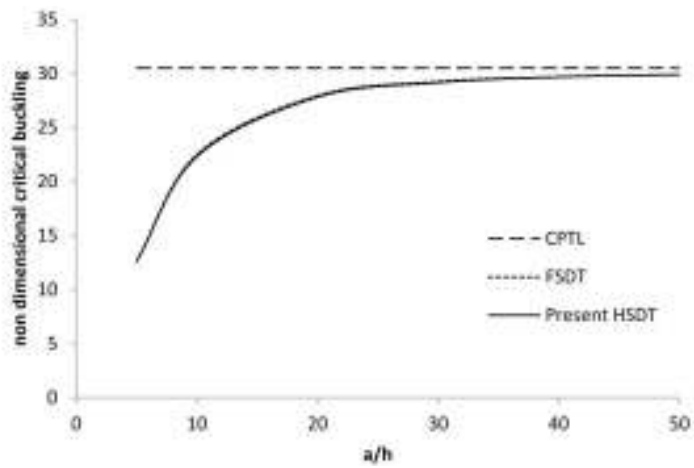


Figure 13: The effect of side-to-thickness ratio on nondimensionlized uniaxial buckling load of simply-supported four-layer (0 / 90 / 0 / 90) square laminates subjected to uniaxial buckling; $E_1/E_2 = 40$.

Number of layers	Source	$\overline{N}$	Error (%)
4	Exact (Noor, 1975)	21.2796	-
	TSDT (Reddy, 2004)	22.5790	6.11
	FSDT (Reddy, 2004)	22.8060	7.17
	RPT (Kim et al., 2009b)	22.5700	6.06
	Present (PSDT)	**22.3306**	**4.93**
	Present (HSDT)	**22.3337**	**4.95**
	Present (SSDT)	**22.3044**	**4.81**
	CLPT	30.3591	42.67
6	Exact (Noor, 1975)	23.6689	-
	TSDT (Reddy, 2004)	24.4596	3.34
	FSDT (Reddy, 2004)	24.5777	3.84
	RPT (Kim et al., 2009b)	24.4581	3.33
	Present (PSDT)	**24.2258**	**2.352**
	Present (HSDT)	**24.2267**	**2.356**
	Present (SSDT)	**24.2264**	**2.355**
	CLPT	33.5817	41.88
10	Exact (Noor, 1975)	24.9636	-
	TSDT (Reddy, 2004)	25.4225	1.84
	FSDT (Reddy, 2004)	25.4500	1.95
	RPT (Kim et al., 2009b)	25.4225	1.84
	Present (PSDT)	**25.1976**	**0.937**
	Present (HSDT)	**25.1975**	**0.936**
	Present (SSDT)	**25.2100**	**0.986**
	CLPT	35.2316	41.13

Table 8: Nondimensionalized uniaxial buckling load of simply-supported asymmetric cross-ply $(0\ /\ 90\ /\ ...)$ square laminates with $(a/h = 10)$ and $E_1/E_2 = 40$.

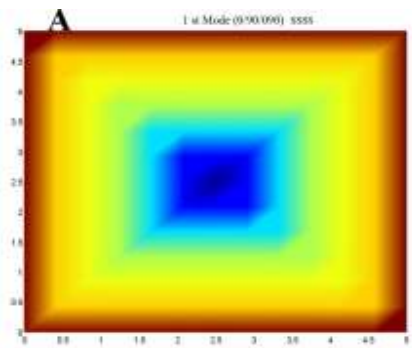


Figure 14: Buckling mode shape of a square laminated composite plate (0/90/0/90) with simply supported boundary conditions and $a/h = 5$.

4 CONCLUSIONS

The finite strip numerical solution and the use of the refined plate theory for orthotropic and laminated composite plates at different boundary conditions have been investigated. Also in this

solution, the results of various transverse shear functions have been compared. The important findings of this analysis can be expressed as follows:

1- In this paper, we employed the four transverse shear functions of PSDT, HSDT, ESDT and SSDT (Table 1). In section 3.2 (Table 5), all four functions are used for the analysis of different plate samples and demonstrated that the non-dimensional buckling loads of the PSDT and HSDT functions are less than those obtained the ESDT and SSDT functions. Therefore in Section 3.1, we only used the PSDT function for analysis.
2- In Section 3.4 (Table 8), it is shown that the results obtained by the PSDT function are closer to the exact solution.
3- The present theory yields more accurate buckling load values than the first-order shear deformation theory.
4- The buckling loads of the hyperbolic transverse shear function has a good accuracy compared with those of the first-order shear deformation theory.
5- The buckling loads of the exponential transverse shear function is usually higher than those of the first-order shear deformation theory.
6- This paper provided many examples for the the analysis of orthotropic plates with different boundary conditions and subjected to uniaxial and biaxial loading situations. Examples of laminated composite plats with different layers and sizes are presented in section 3.4, in all cases good accuracy is observed.
7- The most significant feature of this theory is that it may apply the transverse shear strains across the thickness as parabolic, sinusoidal, hyperbolic and exponential functions. Also, by having fewer unknowns in the equations, this theory enjoys a simpler form which is close to that of the CPT.

References

Abdelaziz, H.H., Atmane, H.A., Mechab, I., Boumia, L., Tounsi, A., Abbas, A.B.E., (2011). Static analysis of functionally graded sandwich plates using an efficient and simple refined theory. Chinese Journal of Aeronautics 24(4): 434-448.

Ambartsumian, S.A., (1958). On the theory of bending plates. Izv. Otd. Tech. Nauk, AN SSSR. 5: 69-77.

Atmane, H.A., Tounsi, A., Mechab, I., Adda Bedia, E.A., (2010). Free vibration analysis of functionally graded plates resting on Winkler-Pasternak elastic foundations using a new shear deformation theory. International Journal of Mechanics and Materials in Design 6(2): 113-121.

Azhari, M., Kassaei, K.H., (2004). Local buckling analysis of thick anistropic plates using complex finite strip method. Iranian Journal of Science & Technology, Shiraz University 28: 21-30.

Bao, G., Jiang, W., Roberts, J.C., (1997). Analytic and finite element solutions for bending and buckling of orthotropic rectangular plates. International Journal of Solids and Structures 34(14): 1797-1822.

Benachour, A., Tahar, H.D., Atmane, H.A., Tounsi, A., Ahmed, M.S., (2011). A four variable refined plate theory for vibrations of functionally graded plates with arbitrary gradient. Composite Part B: Engineering 42(6): 1386-1394.

Benyoucef, S., Mechab, I., Tounsi, A., Fekrar, A., Ait Atmane, H., Adda Bedia, E.A., (2010). Bending of thick functionally graded plates resting on Winkler-Pasternak elastic foundations. Mechanics Composite Materials

46(4): 425-434.

Bui, H.C., Rondal, J., (2008). Buckling analysis of thin-walled sections by semi-analytical Mindlin-Reissner finite strip: A treatment of drilling rotation problem. Thin-Walled Structures 46: 646-652.

Cheung, Y.K., (1976). Finite strip method in structural analysis. Pergamon Press.

Das, Y., (1963). Buckling of rectangular orthotropic plates. Applied Scientific Research 11(1): 97-103.

Dawe, D.J., Roufaeil, O.L., (1978). Buckling of rectangular Mindlin plates. Computers and Structures 15(4): 461-471.

Eisenberger, M., Alexandrov, A., (2003). Buckling loads of variable thickness thin isotropic plates. Thin-Walled Structures 41(9): 871-889.

Ghannadpour, S., Ovesy, H.R., Nassirnia, M., (2012). Buckling analysis of functionally graded plates under thermal loadings using the finite strip method. Computers and Structures 108-109: 93-99.

Harik, I., Ekambaram, R., (1988). Elastic stability of orthotropic plates. Thin-Walled Structures 6(5): 405-416.

Hwang, I., Lee, J., (2006). Buckling of orthotropic plates under various in-plane loads. KSCE Journal of Civil Engineering 10(5): 349-356.

Kaczkowski, Z., (1968). Plates. In: Statical calculations. Arkady, Warsaw.

Kang, J.H., Leissa, A.W., (2005). Exact solutions for the buckling of rectangular plates having linearly varying in-plane loads on two opposite simply-supported edges. International Journal of Solids and Structures 2(14): 4220-4238.

Karama, M., Afaq, K.S., Mistou, S., (2003). Mechanical behavior of laminated composite beam by the new multi-layered laminated composite structures model with transverse shear stress continuity. International Journal of Solids and Structures 40(6): 1525-1546.

Karama, M., Afaq, K.S., Mistou, S., (2009). A new theory for laminated composite plates. Part L: Journal of Materials Design and Applications 223: 53-62.

Kim, S.E., Thai, H.T., Lee, J., (2009a). Buckling analysis of plates using the two variable refined plate theory. Thin-Walled Structures 47: 455-462.

Kim, S.E., Thai, H.T., Lee, J., (2009b). A two variable refined plate theory for laminated composite plates. Composite Structures 89(2): 197-205.

Leissa, A.W., Kang, J.H., (2002). Exact solutions for vibration and buckling of an SS-C-SS-C rectangular plate loaded by linearly varying in-plane stresses. International Journal of Mechanical Science 44(9): 1925-1945.

Levinson, M., (1980). An accurate simple theory of statics and dynamics of elastic plates. Mechanics Research Communications 7: 343-50.

Malekzadeh, P., Shojaee, M., (2013). Free vibration of nanoplates based on a nanlocal two-variable refined plate theory. Composite Structures 95: 443-452.

Mantari, J.L., Oktem, A.S., Guedes Soares, C., (2012). A new higher order shear deformation theory for sandwich and composite laminated plates. Composite Part B: Engineering 43: 1489-1499.

Mantari, J.L., Oktem, A.S., Guedes Soares, C. (2012). Bending response of functionally greded plates by using a new higher order shear deformation theory. Composite Structures 94 (2): 714-723.

Mechab, B., Mechab, I., Benaissa, S., (2012). Analysis of thick orthotropic laminated composite plates based on higher order shear deformation theory by the new function under thermo-mechanical loading. Composite Part B: Engineering 43: 1453-1458.

Mechab, I., Mechab, B., Benaissa, S., (2012). Static and dynamic analysis of functionally graded plates using Four-Variable Refined plate theory by the new function. Composite Part B: Engineering 45(1): 748-757.

Meiche, N.E., Tounsi, A., Ziane, N., Mechab, I., Adda Bedia, E.A., (2011). A new hyperbolic shear deformation theory for buckling and vibration of functionally graded sandwich plates. International Journal of Mechanical

Science 53(4): 237-247.

Mindlin, R.D., (1951). Influence of transverse shear deformation on flexural motions of isotropic, elastic plates. ASME Journal of Applied Mechanics 18(1): 31-38.

Murthy, M.V., (1981). An improved transverse shear deformation theory for laminated composite plates. NASA Technical Paper.

Narendar, S., (2011). Buckling analysis of micro-/nano-scale plates based on two-variable refined plate theory incorporating nonlocal scale effects. Composite Structures 93(12): 3093-3103.

Noor, A.K., (1975). Stability of multilayered composite plate. Fiber Science and Technology 8: 81-89.

Panc, V., (1975). Theories of elastic plates. Prague Academia.

Reddy, J.N., (1984). A simple higher-order theory for laminated composite plates. ASME Journal of Applied Mechanics 51(4): 745-752.

Reddy, J.N., (2004). Mechanics of laminated composite plates and shells. 2nd ed, CRC press.

Reissner, E. (1945). The effect of transverse shear deformation on the bending of elastic plates. ASME Journal of Applied Mechanics 12(2): 69-72.

Ren, J.G., (1990). Bending, vibration and buckling of laminated plates, Handbook of ceramics and composites. vol. I, New York, Marcel Dekker.

Shimpi, R.P., (2002). Refined plate theory and its variants. AIAA Journal 40(1): 137-146.

Shimpi, R.P., Patel, H.G., (2006a). Free vibrations of plates using two-variable refined plate theory. Journal of Sound and Vibration 296(4-5): 979-999.

Shimpi, R.P., Patel, H.G., (2006b). A two variable refined plate theory for orthotropic plate analysis. International Journal of Solids and Structures 43(22-23): 6783-6799.

Soldatos, K.P., (1992). A transverse shear deformation theory for homogenous monoclinic plates. Acta Mechanica 94: 195-220.

Thai, H.T., (2012). A nonlocal beam theory for bending, buckling and vibration of nanobeams. International Journal of Engineering Science 62(1): 56-64.

Thai, H.T., Choi, D.H., (2012a). An efficient and simple refined theory for buckling analysis of functionally graded plates. Applied Mathematical Modelling 36(3): 1008-1022.

Thai, H.T., Choi, D.H., (2012b). A refined shear deformation theory for free vibration of functionally graded plates on elastic foundation. Composite Part B: Engineering 43(5): 2335-2347.

Thai, H.T., Kim, S.E., (2011). Levy-type solution for buckling of orthotropic plates based on two variable refined plate theory. Composite Structures 93(7): 1738-46.

Thai, H.T., Kim, S.E., (2012a). Analytical solution of a two variable refined plate theory for bending analysis of orthotropic Levy-type plates. International Journal of Mechanical Science 54(1): 269-276.

Thai, H.T., Kim, S.E., (2012b). Levy-type solution for free vibration of orthotropic plates based on two variable refined plate theory. Applied Mathematical Modelling 36(8): 3870-3882.

Touratier, M., (1991). An efficient standard plate theory. International Journal of Engineering Science 29(8): 745-752.

Vo, T.P., Thai, H.T., (2012). Vibration and buckling of composite beams using refined shear deformation theory. International Journal of Mechanical Science 62(1): 67-76.

Wang, C., Lim, G., Reddy, J., Lee, K., (2001). Relationships between bending solutions of Reissner and Mindlin plate theories. Engineering Structures 23(7): 838-49.

Zenkour, A.M., (2005). A comprehensive analysis of functionally graded sandwich plates: Part 2-buckling and free vibration. International Journal of Solids and Structures 42(18-19): 5243-5258.

Appendix

Basic function (S_m):

(1) Both ends simply-supported

$$S_m = \sin\frac{\mu_m y}{b} \text{ where } \mu_m = m\pi$$

(2) Both ends clamped

$$S_m = \sin\frac{\mu_m y}{b} - \sinh\frac{\mu_m y}{b} - a_m\left[\cos\frac{\mu_m y}{b} - \cosh\frac{\mu_m y}{b}\right]$$

in which $a_m = \dfrac{\sin\mu_m - \sinh\mu_m}{\cos\mu_m - \cosh\mu_m}$ and $\mu_m = \dfrac{2m+1}{2}\pi$

(3) One end simply-supported and the other end clamped

$$S_m = \sin\frac{\mu_m y}{b} - a_m \sinh\frac{\mu_m y}{b}$$

in which $a_m = \dfrac{\sin\mu_m}{\sinh\mu_m}$ and $\mu_m = \dfrac{4m+1}{4}\pi$

(4) One end clamped and the other end free

$$S_m = \sin\frac{\mu_m y}{b} - \sinh\frac{\mu_m y}{b} - a_m\left[\cos\frac{\mu_m y}{b} - \cosh\frac{\mu_m y}{b}\right]$$

in which $a_m = \dfrac{\sin\mu_m + \sinh\mu_m}{\cos\mu_m + \cosh\mu_m}$ and $\mu_m = \dfrac{2m-1}{2}\pi$